UNDERSTANDING THE HPM GENERATION IN ATMOSPHERIC AIR WITH REFERENCE TO SMALL-SIZE MCG

Mladen M. Kekez

High-Energy Frequency Tesla Inc., (HEFTI), 1200 Montreal Road,
NRC-Site, Building M-51, Ottawa, ON, Canada, K1A 0R6, E-mail: mkekez@hefti.ca, Web: www.hefti.ca

Abstract

The theoretical model of the HPM generation is presented. The model suggests that the peak power can reach the theoretical value of 1.8 GW. The model yields the current waveform supplied by the generator to the HPM emitting structure that operates in atmospheric air. Comparison between the experiment and the theory is given. To get maximum radiating power from the system, it is suggested that the system must be designed to follow the concept of double resonance, put forward by Nikola Tesla.

I. INTRODUCTION

The circuit inductance, $L(t)$ decreases under the influence of the external force of the explosive charge in the MCG. The MCG (also known as the Flux Compression Generator, FCG) produces relatively low voltages, and has a slow release of energy when compared with the requirements needed for the operation of the classical HPM devices. The power-conditioning arrangement is usually required. One of the simplest methods is to employ the opening switch (OS). A simple thin wire/fuse can be both: the OS and the load to the MCG. See Fig. 1.

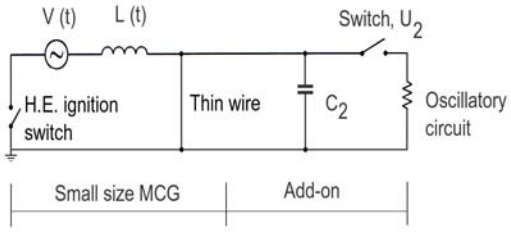

Figure 1. Schematic of small size MCG with the "Add-on" as the power-conditioning stage. The oscillatory circuit generates the RF/HPM radiation. See Ref. [1]

The current flows through the OS during the MCG operation. The thin wire is designed to explode when the current of MCG is to reach its maximum value, I_f and $L(t)$ is at the minimum value, L_f. When the current is interrupted, the electro-magnetic induction voltage impulse of amplitude, V_m is generated. Reinovsky *et al.* [2] have shown that the voltage waveform of the electromagnetic induction takes the shape of the Gaussian function.

If the switch U_2 is open and, if the losses (due to the energy spent to melt the wire and to the onset of unwanted corona discharges) are neglected, Eq. 1 should hold:

$$\frac{L_f I_f^2}{2} = \frac{C_2 V_m^2}{2} \tag{1}$$

Eq. 1 states that the magnetic energy of MCG is converted into the potential energy, $(C_2 V_m^2)/2$. To get the optimum energy transfer it is necessary to use the appropriate value for C_2 in the "Add-on" section of Fig. 1. The right characteristics for the switch U_2 are also needed. After the switch U_2 is closed the energy stored in C_2 is delivered to the load. In Fig. 1 it is assumed that this load is the oscillatory circuit.

Using the exploding wire, Shimomura *et al* [3] found that an output voltage, V_m of 800 kV was obtained when a charging voltage of 15 kV/stage was applied to a 5-stage, 225 J Marx bank. By compressing the energy stored in the coil, the electromagnetic induction voltage was found by Kekez [1] to rise from the initial value at the output of the coil of ≤ 6 kV to reach up to 750 kV in a 6-stage, 92 J Marx generator.

Fortov *et al* [4] used the arrangement similar to that of Fig. 1 in their study of the 10 kJ MCG and have achieved the voltage impulse above 800 kV. The energy of 1-2 kJ was transferred into a high-resistive load. Selemir *et al* [5] suggest that the high voltage pulse is to be created by a two-stage process. The pulse is to be sharpened to a level of ≈ 1 μs by explosive type switches, followed by further application of the OS.

The output voltage up to 800 kV has been achieved by Sun *et al* [6] using electrically exploding switch in their MCG capable of producing more than 20 GW into a 100 Ω resistive-load.

Fig. 1 and Eq. 1 suggest that C_2 charged at voltage, V_m with the switch U_2 can be regarded as an equivalent circuit of the "compact Marx" generator. Therefore, the physics of the HPM generations can be equally studied with the Marx generator instead of using the MCG.

II. FORMULATION OF THE CIRCUITS

To use the energy generated by the MCG, the conventional approach is to attach the classical HPM device such as the Vircator or BWO after the switch U_2. Numbers of excellent papers have been published using this idea.

We were interested to find out whether the part of MCG structure itself can also yield the HPM data that are comparable to the classical HPM devices. Prishchepenko *et al* [11] have originally suggested this idea. The analysis of our data with the MCG-like coil suggests that, the essential features of this approach can be equally obtained with far more simple geometry. It can be shown that the processes taking place with MCG-like helix are similar to that occurring at the output of the generator around the bushing of the generator. See Fig. 2.

When the generator is activated, the voltage front (i.e. electromagnetic wave) propagates between the enclosure of the generator and the central post towards the sphere. Before the spark breakdown takes place between the sphere and the metallic enclosure of the generator, the circuit remains open. The voltage doubles its value at the sphere, because the voltage front sees the end of the open-circuited line. For 10-stage Marx generator charged at 26.5 kV per stage, this voltage value at the sphere is -530 kV. Afterwards the front is reflected back to the generator.

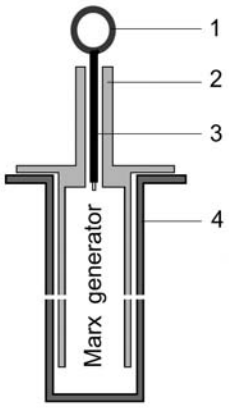

Figure 2. The schematic of the bushing of the Marx generator: (1) is the metallic sphere, (2) plexiglass, (3) central metallic post and (4) is the metallic enclosure of the Marx generator.

To do the analysis of the circuit , the structure of Fig. 2 can be treated as the open-circuited delay line having the characteristic impedance, Z_{00} and the time delay T_{00} that corresponds to the distance, l (≈ length of the post). The central post of the generator with the sphere can also be treated as the short linear antenna. The power radiated can be calculated according to Kraus *et al* [7].

When the plexiglass sleeve surrounding the central post of Fig. 2 is short, the spark breakdown occurs between the sphere and the metallic enclosure of the Marx generator. To measure the conductive component of the current that is entering the metallic enclosure of the generator, the shunt was inserted. To do the theoretical formulation, it became advantageous to insert the thin copper wire ahead of the shunt. See Fig. 3.

The central post with the sphere, #1 on top of it, together with the thin copper wire (thin vertical line) forms the delay line of the characteristic impedance, Z_0. We take that the spark breakdown occurs between the sphere and the top portion of the lead. At the bottom portion of the thin copper wire, the shunt is connected. The other side of the shunt is attached to the metallic enclosure of the generator.

The delay line of Fig. 3 is short-circuited by the spark and can be treated as the loop antenna. The radiated power can be again calculated according to Kraus *et al* [7]

The characteristic impedance of the two-wire delay line, shown in Fig. 3 is given in Eq. 2.

$$Z_0 = \frac{60}{\sqrt{\varepsilon_r}} \ln \frac{D^2}{r_1 r_2} \qquad (2)$$

Here, r_1 and r_2 is the radius of the wires. D is the separation between the wires measured from the axis of the wires.

For $\varepsilon_r = 3$, $r_1 = 3.1$ mm, $r_2 = 0.7$ mm and $D = 17$ mm, Z_0 is 169 Ω. Because the corona discharge is occurring around the thin wire, the effective radius of r_2 may increases as much as 30 mm. In this case for $\varepsilon_r = 1$, $r_1 = 3.1$ mm, and $D = 17$ mm, Z_0 becomes 68 Ω. In the theoretic work, Z_0 varied from 60 to 370 Ω.

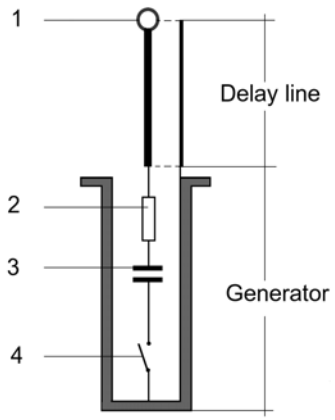

Figure 3. The equivalent circuit of the arrangement shown in Fig. 1: (1) is the sphere, (2) the effective internal impedance of the generator, (3) the erected capacitance of the Marx generator, $C = 0.2$ nF is charged to potential $V = 265$kV and (4) is the ideal ON/OFF switch.

Fig. 4 gives the equivalent circuit of the switch and the loop antenna

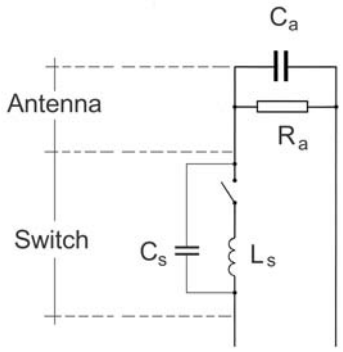

Figure 4.

The spark gap breakdown is presented as the ideal ON/OFF switch that has the inductance, L_s and the electrode capacitance, C_s. After the switch is closed, the loop antenna is taken to have the radiation resistance, R_a and its reactive component, C_a is due to the corona discharge from the thin wire to the ground.

According to Lee, [8] the input impedance of the loop antenna is a strong function of frequency in the range of 0 to 0.9 GHz. His two examples of L-band antennas also indicate that the dependence of the input impedance is relatively modest in the frequency range from 0.96 to 1.21 GHz and R_a has the value of 30 to 70 Ω.

To use the PSpice program, we assume that R_a and C_a are independent of frequency.

III. PSPICE SIMULATIONS OF THE CIRCUIT

A "dry" run was made and the results are given in Figs. 5 and 6.

The erected capacitance of the Marx generator, C is taken to be 1 nF and the generator produces the voltage pulse, V of 300 kV. The energy stored in C ($CV^2/2$) is 45 J.

The characteristic impedance of the delay line, Z_o is assumed to 370 Ω. T_0 (of Z_0) is 0.22 ns. The capacitance of the sphere C_s of 0.5 pF is calculated in regards to the metallic enclosure of the generator rather than to the thin lead of the delay line, because Z_0 is large.

The radiation resistance of the loop antenna, R_a is assumed to be 70 Ω and its reactive component, C_a is taken to be 20 pF.

The spark breakdown is assumed to occur over the dielectric surface in the multi-channel mode enabling L_s to be 1.2 nH.

The internal impedance of the generator, R_i of 1.6 Ω is assumed, because the voltage reflected from the sphere will ionise the gas inside the enclosure of the generator in the vicinity of the last stage of the Marx generator. A large displacement current flowing to the metallic enclosure of the generator supports this glow-like discharge. The effective internal impedance of the generator could become small (< 10 Ω), however in the simulation, R_i varies from 1.6 to 100 Ω.

The main points of the simulation are:

- The current through the ideal switch is in 10 kA range,
- Its FFT has several well defined peaks with the main peak at 5.96 GHz and
- The voltage waveform is of oscillatory form before the switch is closed. Its amplitude is doubled in value to 600 kV in comparison to the voltage applied at the erected capacitance of 300 kV.

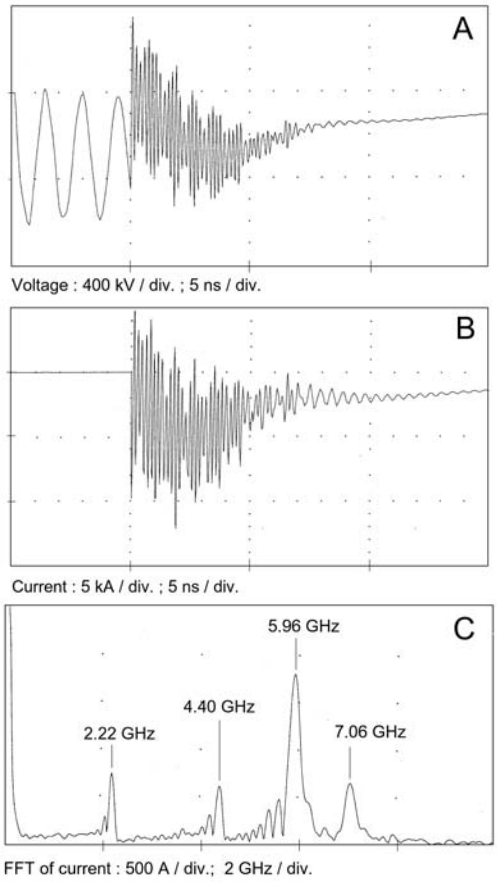

Figure 5. Theoretical data of the voltage and current of the loop antenna: Frame A is the voltage at the sphere in respect to the ground. See Fig. 2. Frame B is the current through the spark gap. Frame C is the FFT of current. The spark gap is taken to close at 5 ns.

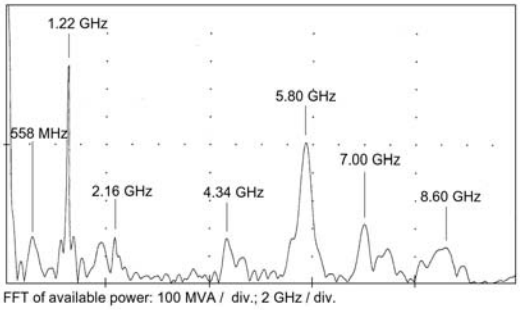

Figure 6. Theoretical data of FFT of the available power: The peaks at 558 MHz and 1.22 GHz are due to linear antenna. Other conditions are as in Fig. 4.

When the combine action of both lines, Z_{00} and Z_0 are considered, it was found that the FFT of the available power (defined as the product of the voltage applied to the sphere times the total current) would produce even more peaks. See Fig. 6.

A far-field expression of the electric field, E_ϕ for a small loop antenna is (after Kraus *et al* [7]):

$$E_\phi = \frac{120\pi I \sin\theta}{r}\frac{A}{\lambda^2} \qquad (3)$$

Here, λ is the wavelength, and I the current, A the area of the loop antenna, and r is the distance. θ is the angle in regards to the vertical axis when the loop is placed in horizontal position.

Eq. 3 gives the relationship between the current, I and λ^2. At high frequencies, the current peaks may be of small amplitude. However, λ^2 may fall even further at higher frequencies. The result is that the field amplitudes, E_ϕ at high frequency can have larger amplitudes than the fields at lower frequency. For short linear antenna, the radiating electric field is proportional to I and inversely proportional only to λ.

The radiation waves at various frequencies will start interacting (or interfering with one another at some distance). Because of the interaction, the electric field probe will record different waveforms when r or θ are changed. For the given distance, it was observed that the experimental data are reproducible. However, with minor changes in the distance, r or angle, θ, the very different waveforms are obtained. For example, the oscilloscope must be set to read "20 to 40 mV" per division to get the readable waveform (and of very complex FFT's) at the distances close to that used to get Fig. 10.

IV. WAVEFORMS

Fig. 7 gives the current waveform supplied by the generator. The current is measured with the shunt made from the tungsten wire, 2 mm in length and inserted to be the part of the delay line, Z_0.

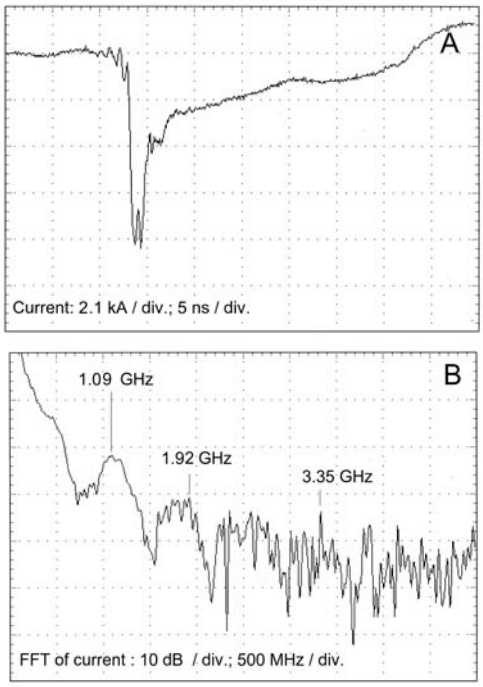

Figure 7. Experimental data of the conductive component of the current supplied by the generator; the displacement component of the current was not measured by the shunt. Frame A shows the current waveform recorded with the shunt with limited bandwidth. Frame B is the FFT of the current shunt. The charging voltage is 26.5 kV per stage. 3-GHz oscilloscope is used.

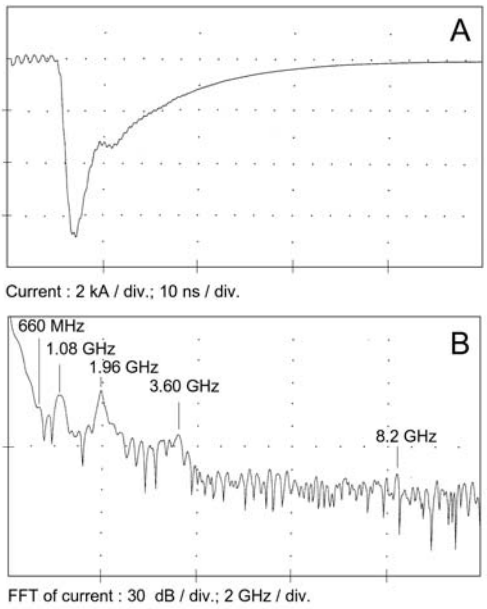

Figure 8. Theoretical data of the conductive current supplied by the generator

The theoretical evaluation of the current is shown in Fig. 8. T_0 of 0.18 ns is used because this value

corresponds to the dimensions in the experimental set up. With Eq. 2, the characteristic impedance of the delay line, Z_0 is estimated to be 90 Ω. The self-reactance of the antenna C_a is of the same value as the one used in Fig. 5. C_a is based on the size of the glow discharge around the thin copper wire of the delay line.

The inductance of the spark gap, L_s of 5 nH is evaluated on the basis of the length of the spark gap channel. The capacitance of the sphere, C_s of 0.5 pF is taken to be the capacitance of the electrodes making the spark gap. The time of 5 ns is taken when the spark gap is closed.

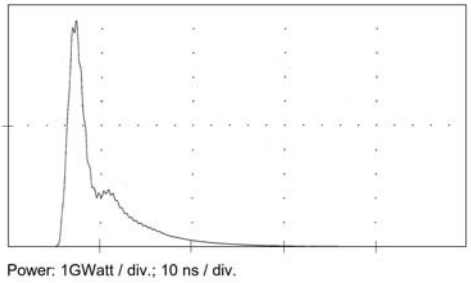

Figure 9. Theoretical waveform of the power radiated by the loop antenna.

The power radiated by the loop antenna is calculated as the product of the radiation resistance of the loop antenna, R_a and the current through it on power two. This result is given in Fig. 9

If the internal impedance of the generator, R_i is 100 Ω, the peak of theoretical waveform of the power will fall to 120 MW and the width of the pulse will increase.

V. RESONANCE

To minimize unwanted interference, the concept of double resonance, put forward by Nikola Tesla was adopted. The concept is that of so called Tesla transformer (coil), with which Tesla has produced a 7 m long spark in his laboratory in the 19 century. The structures given in Figs. 2 and 3 are primary of our Tesla transformer and the space resonator with the reflector (ring/plate) is the secondary of the Tesla transformer. In the resonator the round trip distance, *2d*, is equal to an integral number of wavelengths λ of the wave:

$$2d = N\lambda \text{ where } N = \{1, 2, 3... \} \quad (4)$$

This can also be expressed in terms of frequency:

$$f = N\lambda / 2d \quad (5)$$

The resonator is set so that its frequency, *f* will match one of the main radiation peaks that are arising from the structure (primary) shown in Fig. 3. Through interaction between the resonator (secondary) and the primary, the energy stored in the lines above the frequency *f* (when the resonator is absent) will be transferred to the frequency *f* of the resonator. The result is that the electric field at frequency, *f* may rise up to 100 times and the power density (or power) up to 10^4 times. This depends how well the resonator is designed and what are the losses (Q factor of the oscillatory circuit). The helical antenna can be attached to the resonator to transfer this energy in the form of focused beam on the target.

VI. EXPERIMENTAL DATA OF THE RADIATION

The diameter of the ground-plate of the E-field probe is 15.24 cm. The probe is positioned to be in line with the central metallic #3 shown in Fig. 2. The distance *d*, from the probe to the sphere is 114.9 cm. The experimental data is shown in Fig. 10.

When the result of Fig. 10 is viewed on the faster time scale, Fig. 11 is obtained.

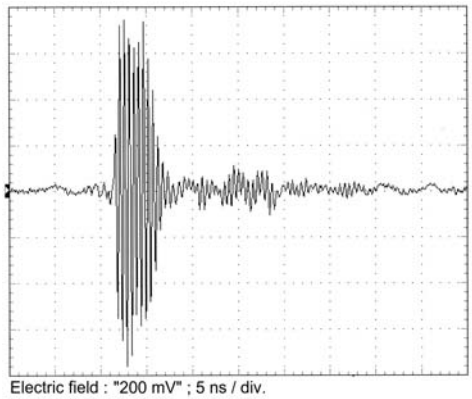

Figure 10. Experimental data of the radiation recorded on 5ns/div. time scale with E-field probe; Experimental conditions are as in Figs. 3 and 7. 3-GHz oscilloscope is used.

Using Eq. 5 and the data given in Fig. 11, we find that the resonance effects are taking place. For 1.95 GHz, *N* is 15 with the error of 0.42%, for 6.95 GHz, *N* = 53+error of 0.45%, for 8.05 GHz, *N* = 60 + error of +1.11% and for 11.95 GHz, *N* = 91 + error of 0.59%.

To confirm that the frequencies above 3 GHz were correct, 16 GHz oscilloscope was used. By placing the probe as close as possible to the place used to get Fig. 10, Fig. 12 was obtained.

Fig. 12 offers support to the theoretical calculation given in Figs. 5 and 6.

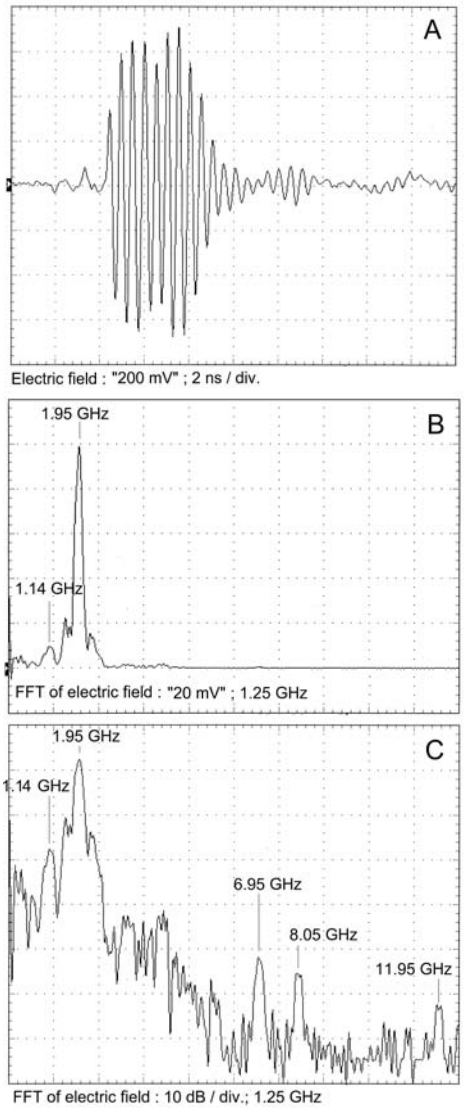

Figure 11. Experimental data of the radiation recorded on 2 ns / div. time scale; Frame A is the electric field of the radiation. Frames B and C are FFT of the frame A. Experimental conditions are as in Fig. 9. 3-GHz oscilloscope is used.

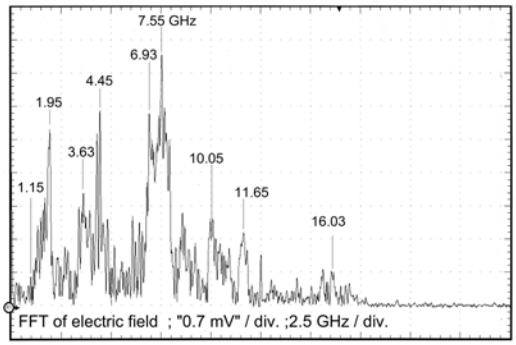

Figure 12. Experimental data: FFT of the electrical field of the radiation; 16-GHz oscilloscope is used.

After numerous experiments, the following points can be noted:

- The resonator acts as the secondary of Tesla double resonance transformer. The resonator is forcing the loop antenna (primary) to radiate at the frequency *f* of the resonator. The energies that were stored in the lines above the frequency *f* are now transferred to frequency *f*. See Figs. 13 and 14.
- The amplitude of the electrical field in the resonator depends on the amount of coupling between the loop antenna and the reflector. In Fig. 13 the reflector is placed above the loop antenna at the distance *d*. The size of the reflector plate is comparable with the metallic enclosure of the Marx generator and the reflector is seeing only the bushing of the generator. A great deal of radiation generated by the loop escape the reflector.
- In Fig. 14, the attempt was made to contain the spreading of the radiation by placing 30 cm long 30 cm diameter tube around the loop antenna. The result is that the field is increased: i.e. the field in Fig. 14 is larger than the field in Fig. 13.
- The field can be further increased by placing the reflector closer to the loop (at smaller value of *N* of Eq. 4). See Fig. 15
- The reflector should be treated as the output lens used in the lasers. For example: 6-stage Marx generator is used to energize the MCG-like helix. It is observed that very small adjustment of the reflector's position; the electric field has been increased 20 times. In these experiments the charging voltage of 13.1 kV is applied to 12 capacitors of 90 nF of the generator. The energy stored in the generator is 92.6 J. *N* factor of Eq. 4 was found to be exactly 7. By comparing Fig. 13 with Fig. 15, we see that the field was increased 5 times and the power density 25 times.
- The mechanical support to hold the lens must be made from dielectrics with the minimum amount of materials. This is because the dielectric also changes the properties of the resonating cavity. There are some indications that are strong spectral lines at frequencies around 50 GHz. By "tuning" the cavity, we are perhaps transferring the energy from these (very high frequency) lines into the low frequencies between 1 and 3 GHz.
- Current work has some resemblance on R&D of the coaxial Vircator. For example Jeon W, *et al.* [9] have increased their total output power by 5 to 7 times by varying the reflector's position.

Their work supports Eq. 4. Yin Y, *et al.* [10] have stressed the importance of the resonant cavity in improving the overall efficiency of the HPM source. It may be interesting to conduct the experiment, where the Vircator structure is placed in the (well defined) laser-like resonant cavity with the two (well designed) lenses. The goal is to see how much the output power will rise.

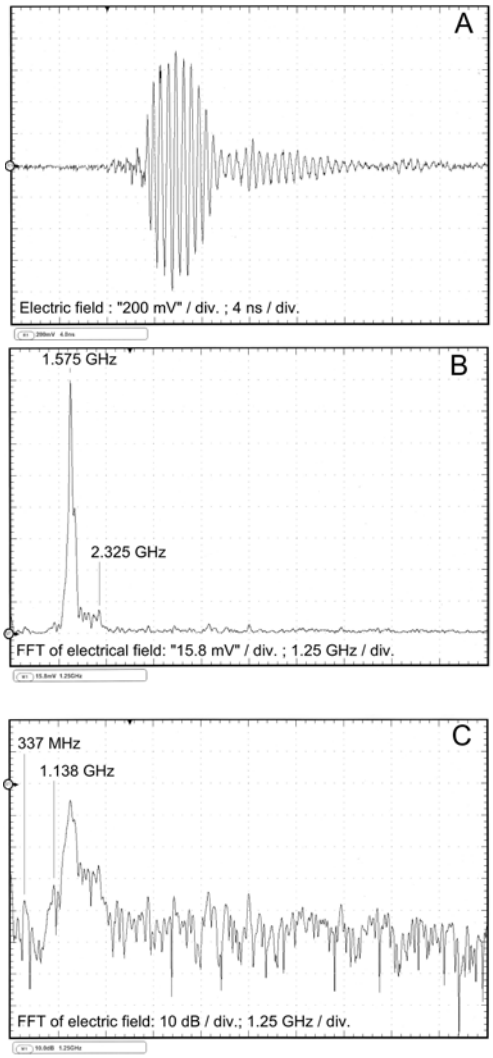

Figure 13. Experimental data: FFT of electrical field of the radiation.

The electric field probe is calibrated using the TEM cell. It was found that "100 mV" stands for 768 V/cm. Fig. 15, Frame A shows that the width of the pulse of 2.35 GHz, δt is 4 ns. During this time the average value of the electric field, E is 23 kV/cm. The power density defined as: $E^2 / (2*Z_0) = (23 \text{ kV/cm})^2 / (2*377\Omega)$ is 0.7 MW/cm^2. To evaluate the energy stored in the resonator it is necessary to obtain the two-dimensional field distribution around the reflector. If, the area of the radiation, A around the reflector is the same as the area of 30 cm diameter tube that encloses the loop antenna, we get for δt = 4 ns and A = 730 cm^2, the energy inside the resonator is 2.9 J at the frequency of 2.35 GHz. For the charging voltage of 26.5 kV/stage, the energy stored in the Mini-Marx generator is 7 J.

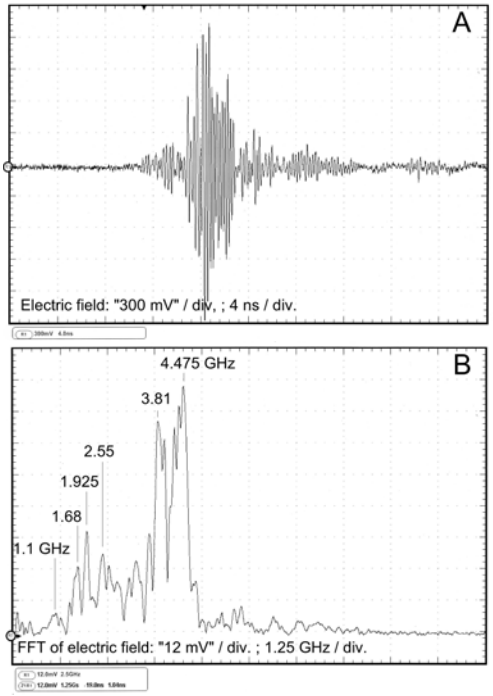

Figure 14. Experimental data: FFT of electrical field of the radiation. The frame B of Fig. 13 should be compared with Fig. 11.

R&D was done to attach the helical antenna to the resonator. 9-stage Marx generator was used in the experiments. The parameters of the system were: the capacitance per stage was 15.6 nF, the charging voltage was 17.5 kV/stage, the energy stored in Marx generator was 21.5 J and the input impedance of the generator was 18 Ω. The generator energized the MCG-like coil. At frequencies of 1.65 GHz, 1.72 GHz and 1.93 GHz the resonance was achieved. The HPM pulses of long (10 to 50 ns) were also recorded. However, the overall gain of the helical antenna (as defined by Kraus [7]) was not yet accomplished

VII. CONCLUSIONS

The Marx generators are used as a surrogate of a small-size MCG to understand the mechanism of the RF/HPM radiation. High-voltage pulses are applied to the open-ended line and later to the short-circuited line. We observe the propagation of the pulses along these lines, and found that the lines are having the function of the vertical monopole and the loop antennas. By placing the plate/ring above these lines, the resonance phenomenon takes place. To get maximum radiating

power, it is suggested that the system must follow the concept of double resonance put forward by Nikola Tesla.

To make further progress in R&D, the use of 20 GHz Tektronix scope is necessary.

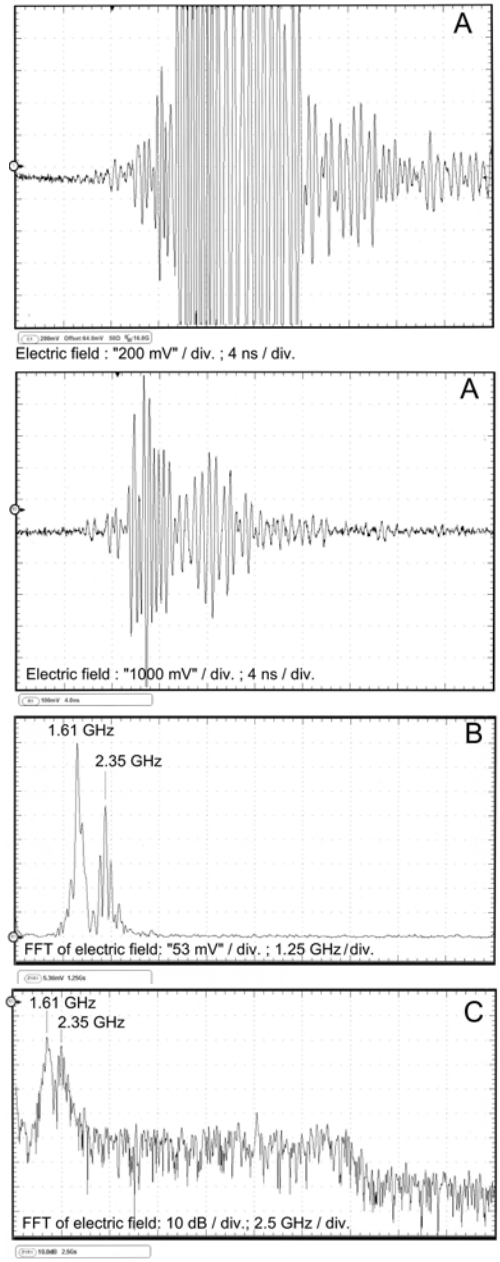

Figure 15. Experimental data of electrical field of the radiation and its FFT's; When the resonance with small *N* number takes place, the amplitude of the electric field rises dramatically (see top frame A). 20 dB attenuator has to be used to get the correct record of the field and its FFT's.

VIII. REFERENCES

[1] M. M. Kekez.. "Energy compression experiments: Simulation of small-size MCG," Proceedings of the 2006 International Conference on Megagauss magnetic field generation and related topics, Santa Fee, NM, USA, 2006, pp. 293-299.

[2] R. Reinovksy, *et al.*, "High voltage power condition system powered by FCG's," Proc. 7th IEEE Conference on Pulsed Power, June 1989, pp. 971–974.

[3] N. Shimomura, *et al.*, "Compact pulsed power generator using a Marx circuit and an exploding write." Jpn. J. Applied Physics, Vol. 40, Jan. 2001, pp. 4199–4204.

[4] V. Fortov, *et al.*, "Multipurpose generator for high power nanosecond H.V. pulses," Proc. 9th International Conference on Megagauss Field and Related Topics, July 2002, pp. 289–295.

[5] V. Selemir, *et al.*, "Conversion of MCG current pulse into H.V. pulse." Proc. 9th International Conference on Megagauss Field and Related Topics, July 2002, pp. 296-301.

[6] Q. Sun, *et al.*, "High-power and high-voltage pulse generation on resistance loads by means of EEMGS" Proc. 10th International Conference on Megagauss Field and Related Topics, July 2004, pp. 201–206.

[7] J.D. Kraus. *Antennas for all applications*, 3rd edition, McGraw-Hill, 2002.

[8] K. S. H. Lee. *EMP Interaction: Principles, Techniques, and Reference Data*, Hemisphere Publishing Co., 1986.

[9] W. Jeon *et al.* "Output characteristics of the HPM generated form a coaxial Vircator with a bar reflector in a drift region." IEEE Transaction on Plasma Science, **34,** pp 937-944, 2006.

[10] Y. Yin, *et al.* "Study of a coaxial Vircator with three mirror quasi-optical resonant cavity." IEEE Transaction on Plasma Science, **34,** pp 18-22, 2006.

[11] A. B. Prishchepenko *et al*, "Dissipation and Diffusion losses in a spiral explosive magnetic generator." Electrichesvo, N. **8.** pp 31-36, 1993.